

GCM SIMULATION OF THERMAL TIDES IN THE MARS ATMOSPHERE

R. John Wilson, NOAA/Geophysical Fluid Dynamics Laboratory, Princeton, NJ (*rjw@gfdl.noaa.gov*), **Don Banfield**, Cornell University, Ithaca, NY, **Dave Hinson**, Stanford University, Stanford, CA, and **Michael D. Smith**, NASA Goddard Space Flight Center, Greenbelt, MD.

Introduction: The thermal tides are planetary-scale gravity waves with periods that are harmonics of the solar day. Tides include westward propagating migrating (sun-synchronous) waves driven in response to solar heating and additional nonmigrating waves resulting from zonal variations in the thermotidal forcing. Nonmigrating tides appear as diurnally varying upslope/downslope circulations within the near-surface boundary layer that, like their migrating counterparts, are able to propagate up to aerobraking altitudes in the lower thermosphere. Thermal tides are particularly prominent in the Mars atmosphere and result in temperature and wind fields with a strong dependence on local solar time (LT) that must be accounted for in interpreting spacecraft observations.

The Mars Global Surveyor (MGS) Thermal Emission Spectrometer (TES) is providing atmospheric temperature profiling with unprecedented latitude and longitude coverage that has provided the basis for characterizing the seasonal evolution of tides and stationary waves [Banfield *et al.*, 2002]. However, the twice-daily observations (2 am and 2 pm LT) are insufficient to unambiguously resolve the sun-synchronous tide nor distinguish between stationary waves and the zonally modulated component of the thermal tide. The MGS data set also includes temperature profiles retrieved from Radio Science (RS) occultations and upper atmospheric (110-170 km) density profiles derived from drag measurements during aerobraking. The RS temperature profiles have much higher vertical resolution than TES retrievals and are particularly valuable for characterizing wave and boundary layer structure [Hinson *et al.* 2001]. These profiles are only available for a limited set of local times, latitudes and longitudes and require additional guidance to provide global context. The accelerometer density observations revealed a surprising degree of longitudinal variation [Keating *et al.* 1998; Wilson 2002] but are representative of a very limited range of local time.

In this presentation, we use Mars general circulation model (MGCM) simulations to provide an interpretation of the temperature structures in the MGS data. The simulated atmospheric fields may be readily decomposed into stationary waves, and eastward and westward propagating thermal tides (and traveling waves) that can be related to the observations. We have also used midlevel (~0.5 mb or 25 km) temperature data from the Viking IRTM instrument [Wil-

son and Richardson 2000] and surface pressure observations at the Viking lander sites [Wilson and Hamilton 1996] for further guidance on thermal tides.

Model Description: The GFDL Mars GCM is based on the GFDL SKYHI terrestrial GCM and an early version of the model is described in Wilson and Hamilton [1996]. The MGCM includes surface and subsurface physics which allow the calculation of realistic surface temperatures; a budget for gaseous and condensed CO₂ which yields a realistic annual cycle of average surface pressure; solar and infrared radiative transfer for gaseous CO₂ and aerosol; aerosol transport which allows for a self-consistent simulation of the aerosol distribution; an inventory of water (regolith, surface frost, water vapor and condensate), and a boundary layer parameterization. Topography and surface thermal inertia are based on MGS observations. The model provides for the transport of water vapor and an arbitrary number of aerosol species that may be used to represent a range of particle sizes and compositions (dust and water ice). Simulations of the annual water cycle and water ice clouds are described in Richardson and Wilson [2002] and Richardson *et al.* [2002] respectively.

We have carried out simulations employing a variety of prescriptions for the injection of dust into the bottom atmospheric layer. The specification of this dust flux provides considerable flexibility in achieving a range of dynamical/thermodynamical states as the atmospheric circulation and the radiatively active dust distribution interactively evolve. For example, the imposition of appropriately large amplitude, episodic dust injection provides a realistic simulation of the peak and decaying stages of major dust storms 1977 (Wilson 1997; Wilson and Richardson 1999) while a weak but steady injection of a spectrum of dust particles can maintain the relatively uniform dust loading indicated by observations in less active seasons.

Thermal Tides: The longitude-time dependence of an arbitrary field in the fixed local reference frame typical for MGS observations may be represented as:

$$A(\lambda, t_T) \sim \sum A_{s,S} \cos[(s-S)\lambda + \mathbf{s}t_T + \delta_{s,S}]$$

where s is the zonal wavenumber, λ is east longitude, S is the temporal harmonic ($S=1$ for the diurnal tide, $S=2$ for the semidiurnal tide), t_T is the local solar time, and $\delta_{s,S}$ is the phase. The relation between universal and local solar time is given by $t = t_{LT} - \lambda$.

Stationary waves are associated with $\sigma = 0$, tides with $s > 0$ ($s < 0$) propagate westward (eastward), and zonally symmetric tides have $s = 0$. The migrating tides ($s = \pm s$) have no longitude dependence in the sun-synchronous reference frame. An observed zonal wave m variation may be due to a combination of a stationary wave, $A_{m,0}$ and a set of nonmigrating tides with $A_{s,s}$, such that $(s - \sigma) = \pm m$. For example, an observed wave 2 variation may be due to the presence of diurnal period westward ($A_{3,1}$) and an eastward propagating ($A_{-1,1}$) diurnal period components as well as contributions from higher temporal harmonics ($A_{0,2}$, $A_{4,2}$, $A_{1,3}$, $A_{5,3}$, ...). Similarly, an observed wave 3 variation is due to contributions from $A_{3,0}$, $A_{-2,1}$, $A_{4,1}$, $A_{-1,2}$, $A_{5,2}$, $A_{0,3}$, ... etc. Other traveling waves possess a spectrum of periods ($0 < \sigma < 1$) that are sufficiently long and are thus less sensitive to local time coverage.

The latitudinal and vertical structure of the atmospheric temperature response depends on both the period and structure of the forcing and on the efficiency of the atmospheric response to a given forcing. In the framework of classical tide theory, the westward propagating diurnal waves ($s = 1, 2, \dots$) may be represented by a series of equatorially confined, vertically propagating waves and vertically trapped waves in the extratropics. The phase and amplitude of the migrating diurnal tide is shown in the top panels of Figure 1 for cases of low (Fig. 1a, $L_s = 358^\circ$) and moderate (Fig. 1b, $L_s = 235^\circ$) dust loading. The simulated diurnal tide response is dominated by a vertically propagating component in the tropics with a vertical wavelength of about 33 km [Wilson and Richardson, 2000]. Shorter vertical wavelengths are obtained for westward nonmigrating tides. Figures 1c and 1d show the corresponding $(T_{2PM} - T_{2AM})/2$ difference fields, which may be compared with the tide fields in Fig. 1e and 1f derived from TES nadir data from the first year of mapping. The panel for $L_s = 235$ corresponds to the period of maximum global mean temperature and tide amplitude following the onset of significant regional dust storm activity at $L_s = 225^\circ$ [Smith et al., 2001]. The vertical wavelength of the tropical diurnal tide is of the order of the vertical smoothing length of the TES nadir retrievals so that the observed amplitudes are likely reduced from the actual atmospheric response. This smoothing likely explains the differences between the observed and simulated tropical temperature differences at $L_s \sim 358$. In particular, the simulation suggests a diurnal difference of approximately 7 K at 0.18 mb rather than the observed ~ 3 K difference. A preliminary analysis of TES limb retrievals indicates an ~ 8 K difference at about 0.1 mb, in close agreement with the simulation. By contrast, the extratropical tide response is characterized by relatively weak phase variation with height and is more representative of dust heating. The differences in tide amplitude between Figs. 1a and 1b

reflect the influence of greater solar heating by dust in the $L_s = 235^\circ$ simulation relative to the $L_s = 358^\circ$ simulation, consistent with the dust opacity retrievals described by Smith et al. [2001].

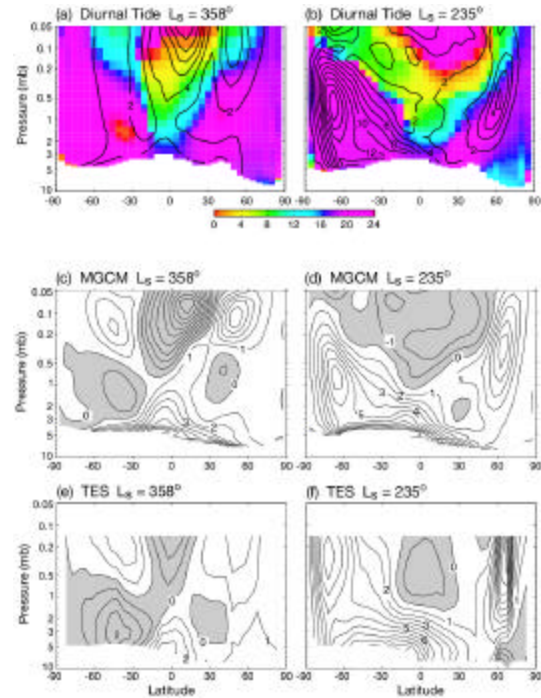


Figure 1: Simulated diurnal tide amplitude and phase for (a) $L_s = 358^\circ$ and (b) $L_s = 235^\circ$. Tide amplitude is contoured at 2K intervals while phase is indicated by color shading. The corresponding $(T_{2PM} - T_{2AM})/2$ fields are plotted in panels (c) and (d). The contour intervals are 1K and negative regions are shaded. The observed TES difference fields are shown in panels (e) and (f). Figure reproduced from Banfield et al. [2002].

Tide theory indicates that the semidiurnal migrating tide response is dominated by a mode with a broad meridional structure and a very long vertical wavelength that efficiently responds to globally integrated dust heating. Leovy and Zurek [1979] showed that the main features of the observed semidiurnal surface pressure oscillation ($S_2(p)$) at Viking lander 1 ($22^\circ N$) can be related to aerosol heating, at least during dusty periods. Figure 2 shows a comparison of the diurnal variation of simulated and observed mid-level temperature ($T_{1.5}$) for the two major dust storms observed by Viking in 1977. Temperatures have been zonally averaged so that the migrating components of the diurnal and semidiurnal tides are evident. The semidiurnal tide is prominent in the tropics while the diurnal tide is quite strong in the southern hemisphere. The evolution of these tide fields and the amplitude of $S_2(p)$ provide strong constraints for estimating the decay of dust heating following the two

Viking dust storms [Wilson and Richardson 1999]. Figure 3 contrasts temperatures observed at the peak of the 2001a global dust storm [Smith et al. 2001] with simulated temperatures consistent with available data corresponding to the peak of the 1977a dust storm observed by Viking. We estimate that the amplitude of the semidiurnal tide for the 2001 storm is ~ 10 K. This tide peaks at 1500 LT (and 0300 LT) so that $(T_{2\text{pm}} + T_{2\text{am}})/2$ temperatures are a biased estimate of diurnal average temperature for these dust storm conditions. Simulations indicate that the semidiurnal temperature amplitude is less than 2 K for more typical conditions.

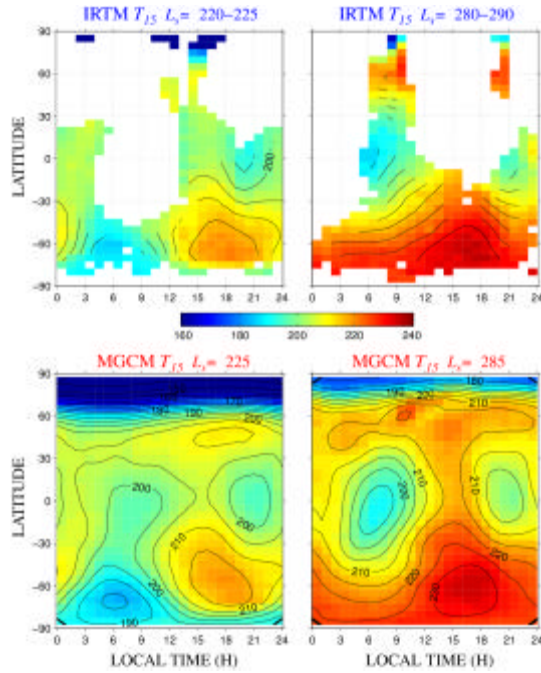


Figure 2: Viking IRTM (top) and MGCM (bottom) T_{15} plotted as a function of latitude and local time for the 1977a (left) and 1977b (right) dust storm periods.

Nonmigrating tides: The most prominent components of the eastward propagating, diurnal period response are the diurnal Kelvin waves (DK1, DK2, ... corresponding to $s=-1, -2, \dots$) which are meridionally symmetric and broad solutions of the Laplace Tidal Equation. DK1 has a vertical structure that closely corresponds to the equivalent barotropic Lamb wave and may be resonantly enhanced [Wilson and Hamilton 1996]. DK2 and DK3 are vertically propagating modes with wavelengths of roughly 90 and 50 km, respectively, and have amplitudes that increase exponentially with height. Long vertical wavelengths render these Kelvin waves less susceptible to thermal dissipation than the shorter westward propagating modes, allowing them to appear prominently in the upper atmosphere [Wilson 2000, Wilson, 2002]. By

contrast, the nonmigrating westward modes include of tropically confined modes with relatively short vertical wavelengths and a second group of mid and high latitude modes that are vertically trapped. Nonmigrating semidiurnal tides also have long vertical wavelengths and evidently contribute to the observed thermospheric density variations [Bougher et al., 2001; Wilson, 2002].

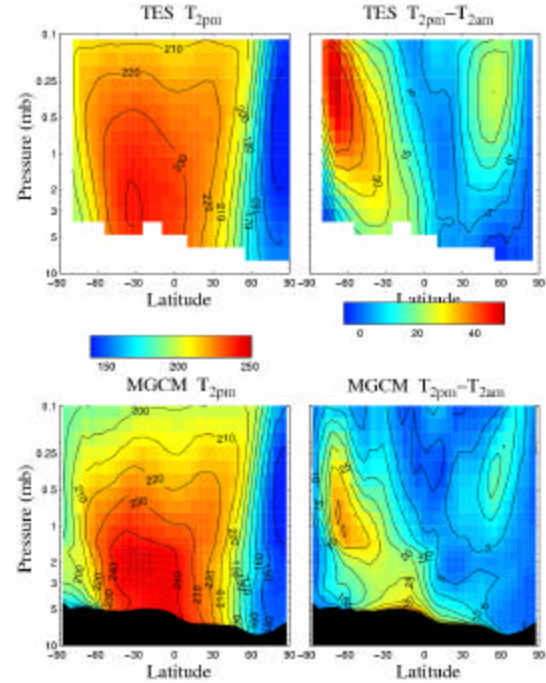


Figure 3: (a) Latitude-height cross-section of 2 pm TES temperature at the peak of the 2001 dust storm at $L_s=205$. (b) Corresponding $T_{2\text{PM}} - T_{2\text{AM}}$ difference field. (c) Simulated 2 pm temperature for the 1977a dust storm. (d) Corresponding difference field.

Systematic seasonal variations in phase and amplitude of the diurnal and semidiurnal surface pressure tides at the two Viking lander sites are consistent with the presence of resonantly enhanced wave 1 diurnal ($A_{-1,1}$ or DK1) and wave 2 semidiurnal ($A_{-2,2}$) Kelvin waves [Wilson and Hamilton 1996]. These waves were shown to be forced by dynamical effects induced by topography.

Wilson [2000] showed that the longitudinal variability of tropical T_{15} synthesized from TES spectra collected during the mapping mission ($L_s=108-350^\circ$) is dominated by nonmigrating thermal tides in low latitudes ($30^\circ\text{S}-30^\circ\text{N}$). A similar finding is also described in Banfield et al. [2002]. The wave 2 and 3 components of tropical temperature in simulations yielding $(T_{2\text{pm}} - T_{2\text{am}})/2$ fields consistent with TES observations were found to be dominated by eastward propagating Kelvin modes with long vertical wavelengths [Wilson 2000].

Figure 4 shows a longitude-height section of simulated zonal wave 2 and 3 components of tropical temperature which may be interpreted as the superposition of eastward propagating Kelvin modes with long vertical wavelengths and westward propagating waves with much shorter wavelengths. Preliminary TES limb retrievals (Figure 4) suggest similar structures, but the shorter westward propagating waves are evidently more strongly attenuated due to the finite vertical resolution. TES nadir results are also consistent with this description, but show the influence of even greater vertical averaging, so that only the long Kelvin waves are evident. Density variations are dominated by the effect of vertically integrated temperature and would tend to reflect the presence of the long Kelvin waves. In fact, measurements obtained during Phase 2 of MGS aerobraking have revealed large amplitude, planetary-scale longitudinal variations in dayside density at 130 km, with zonal waves 2 and 3 being particularly prominent for $\pm 60^\circ$ latitude. *Wilson [2002]* concluded that eastward propagating nonmigrating tides could account for much of the planetary scale wave structure observed in MGS accelerometer density data (in a fixed local time reference). The wave 1 diurnal Kelvin mode (DK1) provides a consistent description of the observed wave 2 structure in density at 130 km, TES temperatures at 25 km and Viking surface pressure data. The observed wave 3 density variation was largely attributed to a wave 2 diurnal Kelvin mode (DK2) in the tropics and an eastward-propagating wave 1 semidiurnal tide at extratropical latitudes.

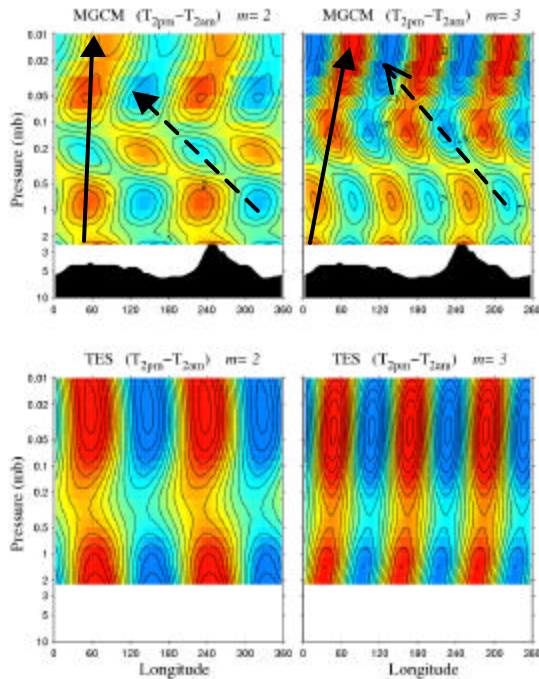


Figure 4: Simulated (top) and observed (bottom) wave 2 (left) and wave 3 (right) components of the

diurnal period nonmigrating tide for $L_s = 150$. Preliminary TES limb data is used in the bottom panels. The contour interval is 1 K. Solid arrows indicate the long Kelvin wave components, DK1 and DK2, in the top left and right panels, respectively.

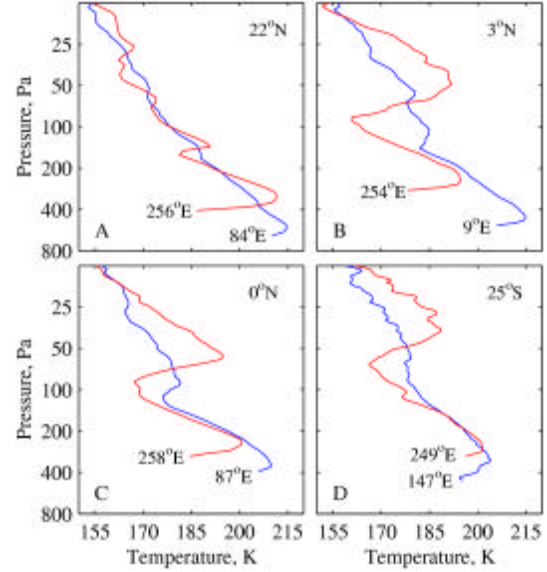


Figure 5: Selected RS profiles at (a) 22 N, $L_s = 140^\circ$, (b) 3 N, $L_s = 147^\circ$, (c) 0 N, $L_s = 148^\circ$, and (d) 25 S, $L_s = 159^\circ$. Red profiles are above Tharsis and blue profiles are at other longitudes. The local time is ~ 0400 LT. Figure from *Hinson and Wilson, 2002*.

MGCM simulations suggest that a rich mix of eastward and westward tide components is likely present at tropical latitudes. Radio Science temperature profiling has revealed dramatic morning (~ 0400 LT) temperature inversions (Figure 5), particularly in the vicinity of the southern Tharsis plateau, that are consistent with the presence of a strong zonal modulation of the vertically propagating diurnal thermal tide [*Hinson and Wilson 2002*]. Simulations have yielded similar temperature inversions that result from a strong local enhancement of the tropical diurnal thermal tide. Figure 6 shows a sequence of simulated temperature profiles in the Tharsis region. The large amplitude tide results from the constructive interference of eastward and westward nonmigrating tides with the migrating diurnal tide. The inclusion of cloud microphysical effects appears to enhance this result. Modeling suggests that these enhancements are associated with diurnally-varying upslope/downslope wind circulations on the flanks of planetary-scale topography. The prominent zonal wave 2 and 3 components shown in Figure 4 contribute significantly to the simulated inversions.

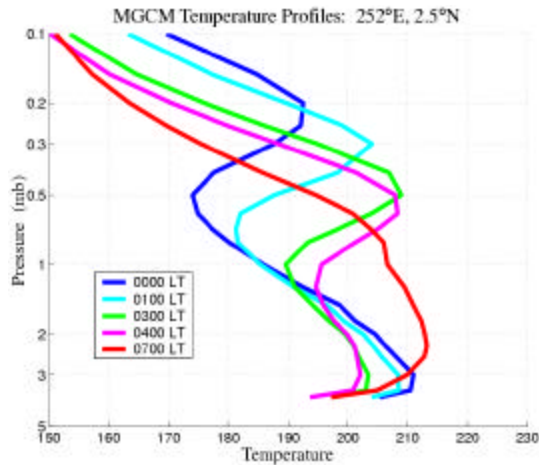


Figure 6: A sequence of temperature profiles showing the descent of an early morning temperature inversion over Tharsis.

In summary, we find that MGCM simulations are able to compensate for the somewhat limited temporal and spatial coverage in remote sensing data. Fitting tide amplitudes to twice-daily temperature fields provides a means of estimating the radiative heating in the atmosphere during dust storm conditions. Modeling has allowed tide modes to be identified and results from different instruments to be related to each other. In short, the MGCM provides a means of interpolating and/or extrapolating observations in a physically consistent manner. The comparison of simulations results with a variety of observational data is a test of the soundness of the underlying parameterizations in the model. Finally, simulations additionally yield the associated dynamical fields, thus providing a means of assessing wind variability and transport capability.

References:

Banfield, D., B.J. Conrath, M.D. Smith, and R.J. Wilson, Forced waves in the martian atmosphere from MGS TES nadir data, *Icarus*, in press, 2002.

Hinson, D.P., G.L. Tyler, J.L. Hollingsworth, and R.J. Wilson, Radio occultation measurements of forced atmospheric waves on Mars. *J. Geophys. Res.*, **106**, 1463-1480, 2001.

Hinson, D., and R.J. Wilson, Tropical temperature inversions and nonmigrating thermal tides on Mars, submitted to *Geophys. Res. Lett.*, August 2002.

Keating, G.M. et al., The structure of the upper atmosphere of Mars: in-situ accelerometer measurements from Mars Global Surveyor, *Science*, **279**, 1672-1676, 1998.

Leovy, C.B. and R.W. Zurek, Thermal tides and Martian dust storms: direct evidence for coupling. *J.*

Geophys. Res., **84**, 2956-2968, 1979.

Richardson, M.I., and R.J. Wilson, Investigation of the nature and stability of the martian seasonal water cycle with a general circulation model, *J. Geophys. Res.*, **107**(E5), 10.1029/2001JE001536, 2002.

Richardson, M.I., R.J. Wilson, and A.V. Rodin, Water ice clouds in the martian atmosphere: General circulation model experiments with a simple cloud scheme, *J. Geophys. Res.*, **107**(E9), 10.1029/2001JE001804, 2002.

Smith, M.D., J.C. Pearl, B.J. Conrath, and P.R. Christensen, One martian year of atmospheric observations by the Thermal Emission Spectrometer, *Geophys. Res. Lett.*, **28**, 4263-4266, 2001.

Smith, M.D., B.J. Conrath, J.C. Pearl, and P.R. Christensen, Thermal Emission Spectrometer observations of martian planet-encircling dust storm 2001a, *Icarus*, **157**, 250-263, 2002.

Wilson, R.J., A general circulation model simulation of the martian polar warming. *Geophys. Res. Lett.*, **24**, 123-127, 1997.

Wilson, R.J., Evidence for diurnal period Kelvin waves in the martian atmosphere from Mars Global Surveyor TES data. *Geophys. Res. Lett.*, **27**, 3889-3892, 2000.

Wilson, R.J., Evidence for nonmigrating thermal tides in the Mars upper atmosphere from the Mars Global Surveyor accelerometer experiment, *Geophys. Res. Lett.*, **29**, 10.1029/2001GL013975, 2002.

Wilson, R.J., and K.P. Hamilton, Comprehensive model simulation of thermal tides in the Martian atmosphere. *J. Atmos. Sci.*, **53**, 1290-1326, 1996.

Wilson, R.J., and M.I. Richardson, Comparison of Mars GCM dust storm simulations with Viking mission observations, Abstract 6234, Fifth International Conference on Mars, Pasadena, CA, 1999.

Wilson, R.J., and M.I. Richardson, The Martian atmosphere during the Viking mission, 1: Infrared measurements of atmospheric temperatures revisited, *Icarus*, **145**, 555-579, 2000.